Gas-Phase Reactions between Hydrocarbons and Metal Oxides: The AlO + CH_4 Reaction from 590 to 1380 K

David P. Belyung and Arthur Fontijn*

High-Temperature Reaction Kinetics Laboratory, The Isermann Department of Chemical Engineering, Rensselaer Polytechnic Institute, Troy, New York 12180-3590

Paul Marshall*

Department of Chemistry, University of North Texas, Denton, Texas 76203-5068

Received: November 16, 1992; In Final Form: February 2, 1993

A recent ab inito study suggested that gaseous metal oxides can directly abstract H atoms from hydrocarbons, but with considerable barriers. To try to confirm the occurrence of such reactions, the title reaction has been studied in a high-temperature fast-flow reactor. The data are well described by the fitting expression k(590–1380 K) = $9.6 \times 10^{-39}(T/\mathrm{K})^{7.96} \exp(2468\ \mathrm{K}/T)$ cm^3 molecule^{-1} s^{-1}, with 2σ precision limits varying with temperature from ±4% to ±12%. The corresponding 2σ accuracy limits are about ±25%. Comparison of this result to further ab initio and conventional transition-state theory calculations suggests that direct abstraction indeed can occur at the higher temperatures but that one or more other channels, possibly involving AlO insertion into a C–H bond, dominate in the initial attack step. The potential implications of this work for catalytic conversion of methane to higher hydrocarbons are considered.

Introduction

In a recent ab initio study Børve and Pettersson[1] predicted that some gaseous metal oxides, LiO, MgO, and AlO, can directly abstract an H atom from methane to produce methyl radicals. Such exothermic reactions have not been observed in the gas phase, and their studies suggested these to have considerable barriers, 25–67 kJ mol^{-1}. However, solid metal oxides have been found to be effective catalysts for H abstraction from methane, leading to C_2H_4 and C_2H_6 in significant yields,[2] a process of considerable commercial promise. The basis for this catalytic reaction has been strongly suggested to be the surface reaction of the O^- ion to remove a hydrogen atom, a process which appears to proceed to a significant degree only above about 1000 K.[3] Theoretical studies of cluster models of the MoO_3 oxide structure have supported this hypothesis.[4] If the occurrence of the gas-phase processes could be experimentally confirmed, it would not only establish a new class of reactions but also could lead to a better understanding of the heterogeneous catalytic processes. We therefore decided to investigate one of these suggested reactions:

$$\mathrm{AlO} + \mathrm{CH_4} \rightarrow \mathrm{AlOH} + \mathrm{CH_3} \qquad (1)$$

for which ΔH° = –27 kJ mol^{-1}.[5,6] While this reaction has a higher predicted barrier than those of the other oxides,[1] we have had extensive experience with the study of the gas-phase reactions of AlO at temperatures up to 1600 K in HTFFRs (high-temperature fast-flow reactors)[7] and therefore selected this oxide.

Technique

The HTFFR facility used in this work and the data handling procedures have been previously described.[7] Briefly, a vertical mullite (McDanel MV-30) reaction tube (60 cm long, 2.2 cm i.d.) is heated to the desired temperature by columns of resistively heated SiC rods inside an insulated, water-cooled vacuum housing. Al vapor is produced by resistively heating an Al-wetted W coil in a flow of Ar carrier gas. A trace of oxidizer, 0.5% N_2O or 5% O_2 in Ar, at ≈4×10^{-3}% of the main Ar flow, is passed through a Pt side tube to a location just downstream from the vapor source to rapidly convert Al to AlO.[8-10] Further downstream CH_4/Ar mixtures at flow rates of 4–8% of the main Ar flow rate are introduced through a movable inlet. Rate coefficient measurements are made under pseudo-first-order conditions, [AlO] ≪ [CH_4], in the stationary inlet mode,[11] at reaction zone lengths of 10 or 20 cm.

Relative AlO concentrations were monitored by laser-induced fluorescence (LIF) using a pulsed Lambda Physik EMG 101 excimer/FL 2002 dye laser in combination with a KDP doubling crystal. Two transitions $B^2\Sigma$–$X^2\Sigma$ and $C^2\Sigma$–$X^2\Sigma$ were used. In the former, AlO is pumped on the 464.8-nm (1,0) band and the fluorescence is observed through a 482-nm (20-nm fwhm) interference filter, i.e., mainly at the 486.6-nm (1,1) band.[12] The $B^2\Sigma$–$X^2\Sigma$ system could only be used up to 1200 K because of interference by the background radiation from the reactor walls. For measurements above 1200 K and some checks at lower temperatures, the $C^2\Sigma$–$X^2\Sigma$ (0,0) transition at 302.2 nm[12] was used in combination with a 301-nm (11-nm fwhm) interference filter. The fluorescence was detected by an EMI 9813QA photomultiplier tube, connected to a Data Precision Analogic 6000/620 100-MHz transient digitizer.

The gases used were 99.998% Ar from the liquid Ar (Linde), 0.5% N_2O (99.99%) in Ar (99.999%) from Matheson, 5% O_2 (99.99%) in Ar (99.995%) from Scott, and CH_4 (99.99%) from Matheson.

Results

Plots of $\ln[\mathrm{AlO}]_{\mathrm{relative}}$ versus [CH_4] yield straight lines with slopes $-kt$, where t is reaction time. For each individual measurement, k and σ_k were determined by a weighted linear regression.[11,13] The k values and the experimental conditions under which they were obtained are summarized in Table I. The measurements may be seen to be independent of the following: pressure varied from 13.1 to 63.3 mbar, corresponding to total concentrations [M] from 8.0×10^{16} to 6.4×10^{17} molecules cm^{-3}; average gas velocity $\bar{v}$ varied from 12 to 98 m s^{-1}; reaction zone length selected at 10 or 20 cm; initial fluorescence intensity F (a measure of initial [AlO]) varied from 9 to 65 in arbitrary units. The temperature range covered is 590–1380 K. The lower limit was determined by the heating effect of the Al vaporizer, and the upper limit by the dissociation of CH_4. An Arrhenius

0022-3654/93/2097-3456$04.00/0

TABLE I: Summary of Rate Coefficient Measurements on the AlO + CH_4 Reaction[a]

reaction zone length (cm)	P (mbar)	[M] (10^{17} cm $^{-3}$)	$[CH_4]_{max}$ (10^{15} cm $^{-3}$)	F[b]	$\bar{V}$ (m s $^{-1}$)	T (K)	$k \pm \sigma_k$ (cm^3 molecule $^{-1}$ s $^{-1}$)
20	26.7	2.1	9.4	17	32	913	4.42 ± 0.33 (−14)[c,d]
20	26.5	2.1	9.4	17	33	912	4.93 ± 0.41 (−14)[d]
20	43.3	3.3	10.3	24	29	928	3.19 ± 0.31 (−14)[d]
20	20.0	1.5	4.8	33	62	932	5.22 ± 0.63 (−14)[d]
20	20.0	1.5	4.8	24	62	935	6.78 ± 0.93 (−14)[d]
20	15.5	1.0	5.0	22	98	1083	1.67 ± 0.21 (−13)[d]
20	15.5	1.0	5.0	20	98	1083	1.83 ± 0.21 (−13)[d]
20	13.1	0.8	4.4	30	90	1135	1.76 ± 0.23 (−13)[d]
20	17.2	1.1	3.8	47	68	1098	1.72 ± 0.21 (−13)[d]
20	17.2	1.1	3.8	32	68	1102	1.75 ± 0.17 (−13)[d]
20	28.9	1.9	4.7	38	48	1103	1.09 ± 0.12 (−13)[d]
20	19.2	1.2	5.8	41	56	1139	1.58 ± 0.19 (−13)[d]
20	16.7	1.1	4.9	64	67	1144	1.81 ± 0.22 (−13)[d]
20	20.1	1.6	9.9	53	46	882	3.30 ± 0.53 (−14)[d]
20	36.7	2.6	4.4	30	29	1001	8.15 ± 0.90 (−14)[d]
20	30.4	2.1	5.8	41	33	1051	8.53 ± 0.79 (−14)[d]
20	32.8	2.2	5.1	38	31	1053	1.11 ± 0.08 (−13)[d]
10	32.8	2.3	8.5	35	30	1031	8.82 ± 0.97 (−14)[d]
10	36.3	2.5	9.4	32	28	1034	8.62 ± 0.81 (−14)[d]
10	19.6	1.4	6.4	64	51	1034	1.43 ± 0.16 (−13)[d]
10	19.6	1.4	7.7	63	51	1037	9.28 ± 1.07 (−14)[d]
20	19.6	1.3	5.0	54	52	1061	1.28 ± 0.14 (−13)[d]
20	19.6	1.3	5.0	53	52	1063	1.29 ± 0.15 (−13)[d]
20	31.7	2.3	7.0	48	37	985	7.38 ± 0.53 (−14)[d]
20	33.6	2.5	7.5	34	35	982	7.22 ± 0.55 (−14)[d]
10	34.3	2.6	9.6	37	34	961	7.91 ± 0.69 (−14)[d]
10	34.3	2.6	9.5	39	34	963	8.18 ± 0.66 (−14)[d]
10	34.3	2.6	7.4	29	44	962	7.11 ± 0.63 (−14)[d]
10	34.3	2.6	7.4	24	44	961	8.19 ± 0.85 (−14)[d]
20	34.4	2.5	5.7	25	46	1000	1.09 ± 0.09 (−13)[d]
20	34.4	2.5	5.7	23	46	1003	1.09 ± 0.09 (−13)[d]
20	24.1	2.1	13.7	26	38	827	2.10 ± 0.21 (−14)[d]
20	24.9	2.5	18.4	28	29	721	1.16 ± 0.15 (−14)[d]
20	24.9	2.5	18.1	24	29	734	1.34 ± 0.14 (−14)[d]
10	25.1	2.5	18.6	28	28	717	1.31 ± 0.12 (−14)[d]
10	25.7	2.5	18.8	28	28	734	1.65 ± 0.22 (−14)[d]
10	36.0	3.3	15.5	52	34	781	2.67 ± 0.32 (−14)[d]
10	35.7	3.3	15.2	38	35	795	3.12 ± 0.39 (−14)[d]
20	16.0	1.2	5.6	53	58	945	7.05 ± 0.83 (−14)[e]
20	16.0	1.2	4.5	35	58	953	7.84 ± 0.97 (−14)[e]
10	16.3	1.3	6.9	39	57	938	1.10 ± 0.12 (−13)[e]
10	16.3	1.3	8.1	65	57	942	1.07 ± 0.14 (−13)[e]
10	21.2	2.4	14.0	34	28	651	1.44 ± 0.18 (−14)[e]
10	39.5	4.3	17.1	9	15	660	1.62 ± 0.20 (−14)[e]
10	39.5	4.3	17.2	9	15	663	1.99 ± 0.14 (−14)[e]
20	34.1	4.1	21.1	42	19	602	5.60 ± 0.64 (−15)[e]
20	34.0	4.0	17.1	30	19	618	9.95 ± 1.27 (−15)[e]
20	34.0	3.9	16.9	25	19	628	1.02 ± 0.13 (−14)[e]
20	53.1	5.3	6.2	9	21	727	2.11 ± 0.23 (−14)[e]
20	24.5	2.9	20.6	15	19	603	7.78 ± 0.91 (−15)[e]
20	24.5	2.9	20.0	27	20	621	8.11 ± 0.65 (−15)[e]
20	14.3	1.7	11.0	33	24	598	6.71 ± 0.77 (−15)[e]
20	14.3	1.7	11.1	20	23	591	6.23 ± 0.78 (−15)[e]
20	63.3	6.4	9.9	11	20	718	1.72 ± 0.20 (−14)[e]
20	15.3	1.4	8.7	34	37	780	2.40 ± 0.26 (−14)[e]
20	15.3	1.4	8.8	40	37	770	2.43 ± 0.31 (−14)[e]
20	21.9	1.8	5.9	25	33	893	4.94 ± 0.54 (−14)[e]
20	56.0	4.8	4.7	23	20	845	3.02 ± 0.31 (−14)[e]
20	13.7	1.2	4.7	20	55	846	4.64 ± 0.53 (−14)[e]
20	13.7	1.2	4.7	16	56	853	3.87 ± 0.47 (−14)[e]
10	14.1	1.2	7.0	24	56	866	5.81 ± 0.75 (−14)[e]
20	44.5	2.3	1.1	19	30	1374	4.57 ± 0.32 (−13)[e]
20	44.7	2.5	1.2	20	28	1380	3.49 ± 0.34 (−13)[e]
20	41.7	4.5	7.4	32	13	668	1.46 ± 0.11 (−14)[f]
20	41.6	4.6	7.5	45	12	650	1.36 ± 0.10 (−14)[f]
20	53.9	5.3	6.8	62	14	736	1.71 ± 0.11 (−14)[f]
20	54.3	5.6	8.3	65	13	707	1.68 ± 0.14 (−14)[f]
20	54.3	5.7	8.5	58	13	686	1.45 ± 0.11 (−14)[f]
20	17.5	1.0	1.5	40	60	1232	3.44 ± 0.37 (−13)[e]
10	24.1	1.4	2.0	37	46	1283	5.07 ± 0.44 (−13)[e]
10	24.1	1.3	2.0	37	47	1296	5.87 ± 0.50 (−13)[e]
20	24.0	1.3	1.3	38	48	1317	4.52 ± 0.35 (−13)[e]
20	24.0	1.3	1.3	39	48	1324	5.21 ± 0.44 (−13)[e]

[a] The measurements are reported in the sequence in which they were obtained. [b] In arbitrary units. [c] Should be read as (4.42 ± 0.33) × 10 $^{-14}$. [d] Data obtained by using the $C^2\Sigma$–$X^2\Sigma$ transition and an alumina ring inlet. [e] Data obtained by using the $C^2\Sigma$–$X^2\Sigma$ transition and a quartz ring inlet. [f] Data obtained by using the $B^2\Sigma$–$X^2\Sigma$ transition and a quartz ring inlet.

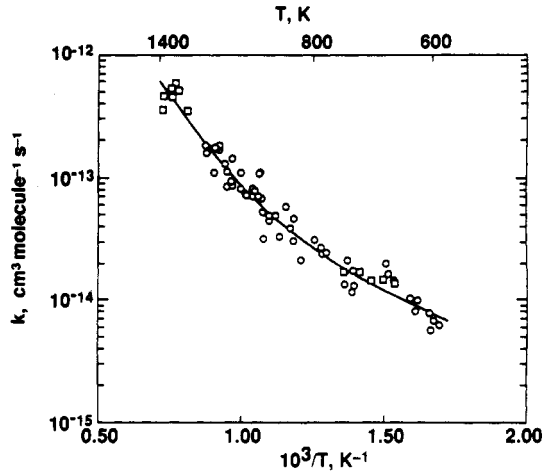

Figure 1. Arrhenius plot of the rate coefficient data of the AlO + CH_4 reaction: □, 5% O_2 used as AlO precursor; ○, 0.5% N_2O used as AlO precursor.

plot of these data, Figure 1, shows strong curvature. Several different expressions were tried to fit the ln k versus T^{-1} data. Using Marquardt's method,[14] a regression fit to a $k(T) = A(T/\mathrm{K})^n \exp(-B/T)$ expression yields

$$k(590\text{–}1380\ \mathrm{K}) = 9.6 \times 10^{-39}(T/\mathrm{K})^{7.96} \times \exp(2468\ \mathrm{K}/T)\ \ \mathrm{cm^3\ molecule^{-1}\ s^{-1}} \quad (2)$$

Equation 2 must be seen as a fitting expression only, as the numbers are unrealistic for a single channel reaction. This $k(T)$ expression most likely indicates competition between several reaction channels. We next attempted a similar regression for a double-exponential expression $k(T) = A \exp(-B/T) + C \exp(-D/T)$, which yielded

$$k(590\text{–}1380\ \mathrm{K}) = 2.0 \times 10^{-10} \exp(-8299\ \mathrm{K}/T) + 4.2 \times 10^{-13} \exp(-2402\ \mathrm{K}/T)\ \ \mathrm{cm^3\ molecule^{-1}\ s^{-1}} \quad (3)$$

This fitting expression also does not seem to be representative of individual actual reaction paths, because of the high preexponential of the first term. This term appears too large for a metathesis reaction between a diatomic radical and a molecule.[15] While molecular insertion reactions, e.g., of singlet CH_2 and SiH_2, are known with A factors of this magnitude, these reactions proceed with an activation energy close to zero.[16-18]

Calculating the uncertainties of these fitting expressions by combining[19] variances and covariances, similarly as in our earlier studies,[7] yields precision limits of ±4% to ±12% for eq 2 and of ±5% to ±12% for eq 3, depending upon temperature. Both expressions lead to essentially equal accuracy limits of ±23% to ±26%, when combined with a ±10% uncertainty in the reactor flow profile[11,20] and ±20% for potential systematic errors. The simpler expression (2) is therefore preferred for the present temperature range.

Discussion

There has been one previous attempt to observe reaction 1. In that room temperature study no reaction could be detected, and an upper limit for the rate coefficient of 5×10^{-14} cm³ molecule⁻¹ s⁻¹ was derived.[8] Equations 2 and 3 suggest much lower values; hence, the results do not contradict one another.

The activation energies, i.e., the local slopes of the Arrhenius plot, Figure 1, reach the 67 kJ mol⁻¹ calculated by Børve and Pettersson[1] only at the highest temperatures investigated. For example, from eq 2 these energies are 46, 59, 66, and 71 kJ mol⁻¹ at 1000, 1200, 1300, and 1380 K, respectively. Also, the fitting expressions suggest that the reaction follows several paths. Further mechanistic considerations thus appear in order. To this end we first assess the likely importance of H-atom abstraction.

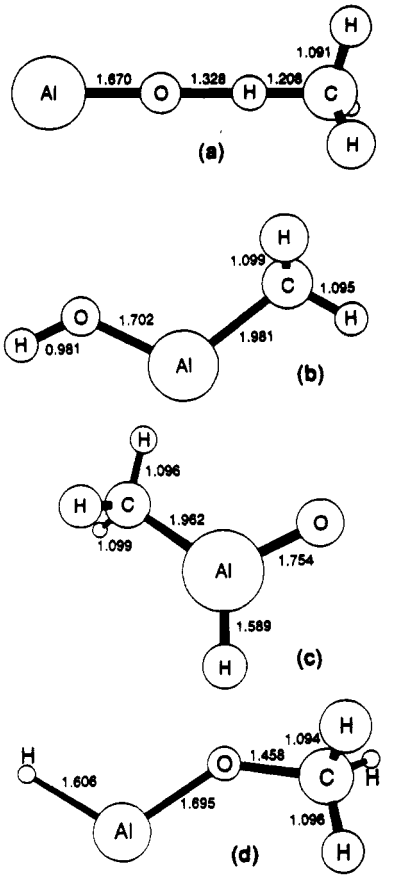

Figure 2. MP2/3-21G(*) structures of (a) C_{3v} TS for H-atom abstraction by AlO from CH_4, ∠AlCH = 106.6°; (b) C_s CH_3AlOH adduct, ∠AlOH = 128.8°, ∠OAlC = 116.2°, ∠AlCH = 112.2°, 109.4°(2); (c) C_s CH_3-Al(O)H adduct, ∠OAlH = 113.7°, ∠HAlC = 127.2°, ∠CAlH = 112.4°, 110.3°(2); (d) C_s CH_3OAlH adduct, ∠HAlO = 114.7°, ∠AlOC = 138.2°, ∠OCH = 112.2°, 109.5°(2). Distances are in 10^{-10} m.

Børve and Pettersson carried out a partial CASSCF optimization of an assumed C_{3v} transition state (TS) but did not obtain enough information to predict rate coefficients. In order to estimate these, we have analyzed abstraction by conventional transition-state theory (CTST), which requires vibrational and rotational data to estimate the partition function of the TS. Accordingly, we reoptimized the complete TS structure, at the MP2/3-21G(*) level,[21] and obtained the vibrational frequencies. The geometry is shown in Figure 2a and confirms their[1] work; the frequencies are 1574i, 175(2), 441(2), 570, 1030, 1357(2), 1394, 1561(2), 3109 and 3226(2) cm⁻¹. For an energy barrier at 0 K (i.e., including zero-point energy, ZPE) of E_0, the CTST abstraction rate coefficient is

$$k(590\text{–}1380\ \mathrm{K}) = 1.43 \times 10^{-22}(T/\mathrm{K})^{3.30} \times \exp(-940\ \mathrm{K}/T) \exp(-E_0/RT)\ \ \mathrm{cm^3\ molecule^{-1}\ s^{-1}} \quad (4)$$

Preliminary estimates showed that quantum mechanical H-atom tunneling has little effect when $k \gtrsim 1 \times 10^{-14}$ cm³ molecule⁻¹ s⁻¹. Agreement between eqs 2 and 4 at 825 K, the midpoint of the range of T^{-1} investigated, is obtained when $E_0(4) = 12.4$ kJ mol⁻¹. This yields $k(1380\ \mathrm{K})$ within 5% of the experimental value, while $k(590\ \mathrm{K})$ is too small by a factor of 2.3. Though accord at low temperatures might be improved by adjustment of the TS frequencies, the fitted $E_0(4)$ is much lower than the $E_0(1) = 67$ kJ mol⁻¹ from the earlier ab initio estimate.[1] Use of that value together with the observed total AlO removal rate coefficient, eq 2, implies a branching ratio for direct abstraction of about 9×10^{-3} at 1380 K and about 6×10^{-6} at 590 K. In order to estimate the uncertainty in the $E_0(1)$ value that Børve and Pettersson derived at the CCI + Q level of theory, we compare their estimates of $\Delta H°$ for reaction 1 and the Li and Mg analogues[1] with the

experimental values.[5,6] The mean error is about ±25 kJ mol^{-1}, which is a minimum estimate of the uncertainty in $E_0(1)$. We also allow for a possible factor of 3 uncertainty in the TS partition functions. These uncertainties imply that branching ratios for direct abstraction, i.e., without formation of an intermediate bound complex, as large as 0.23 at 1380 K and 0.003 at 590 K cannot be excluded, but another reaction channel, which is totally dominant at the lower temperatures, is definitely indicated.

The alternative abstraction channel leading to HAlO + CH_3 would be 192 ± 93 kJ mol^{-1} endothermic[5,6] and can on that basis be excluded from further consideration. The likelier prospects for further channels involve additions of AlO to CH_4. Particularly, insertion of AlO (a doublet species) into a C–H bond offers an intriguing prospect, by analogy to the suggested insertion of Al and other group 13 doublet ground-state atoms into such bonds.[22,23] To test this, we have employed theoretical methods to characterize possible insertion products and estimated the likely pressure dependence of these to see whether they are consistent with our observations. Ab initio geometries of three potential insertion species obtained by means of MP2/3-21G(*) theory are shown in Figure 2b–d. Structure d was previously proposed as the product of insertion of Al into CH_3OH,[24] similar to such insertion into H_2O.[24,25] To confirm that these structures are true energy minima, we calculated the vibrational frequencies, which are all real.[26] These frequencies are also used to derive the zero-point energy (ZPE), to obtain the temperature dependence of the enthalpies in the kinetic calculations outlined below. The enthalpies of CH_3AlOH, $CH_3Al(O)H$, and CH_3OAlH, relative to AlO + CH_4 at 0 K, are predicted at the MP4SDQ/6-31G*+ZPE//MP2/3-21G(*) level to be −166, −46, and −87 kJ mol^{-1}, respectively.[27] Equilibrium constant calculations with these enthalpies indicate that CH_3AlOH is stable under our experimental conditions, that the second adduct is too weakly bound to be a significant final sink for AlO, and that formation of the third adduct cannot be ruled out at the lowest temperatures studied. There is a possibility that these adducts decompose to new products. For example, CH_3AlOH might dissociate to AlOH + CH_3, perhaps with a lower overall energy barrier than proposed for direct abstraction.

Next, the likely pressure dependence of AlO + CH_4 → CH_3AlOH at 825 K was investigated by means of QRRK theory.[28] The addition rate coefficient is predicted to be within 25% of the high-pressure limit at 15 mbar of Ar and would show only a small pressure variation over the experimental range with assumed Arrhenius parameters for insertion of $A = 10^{-12}$ cm^3 molecule^{-1} s^{-1} and $E_a = 0$. This is consistent with the lack of an observed pressure dependence of the experimental rate coefficients. If there were a significant barrier to insertion ($E_a > 0$), then dissociation of the excited adduct back to AlO + CH_4 would be less competitive with collisional stabilization and the predicted rate coefficients would be even closer to the high-pressure limit. The observed pressure independence is also consistent with a mechanism where the adduct fragments to new products before stabilization. Further QRRK calculations suggest that formation of any adduct, which is sufficiently thermodynamically stable to be significant in our experiments, will have a rate coefficient that is in the falloff region or close to the high-pressure limit.

Conclusions

These experiments are in accord with the suggestion by Børve and Pettersson[1] that gas-phase reactions between AlO and CH_4 occur and may provide insight in the heterogeneous catalytic conversion of methane to C_2 hydrocarbons. However, use of their calculated barrier suggests that the branching ratio for direct abstraction is small and therefore that other reaction channels are important. Our calculations demonstrate that insertion leading to CH_3AlOH is a reasonable candidate for the initial step, although other channels are not excluded. The insertion products (Figure 2b–d) might model the products of dissociative adsorption of CH_4 onto an alumina catalyst, where their energies are likely to differ from gas-phase values. More detailed experimental and theoretical investigations of the present reaction system, as well as of other metal oxide–hydrocarbon reactions, are needed to obtain an understanding of this new class of gas-phase reactions and their potential importance for methane conversion.

Acknowledgment. The experimental work was performed at Rensselaer under AFOSR Grants F49620-92-J-0172 and F49620-92-J-0346, and the theoretical study was done at the University of North Texas with support from the Robert A. Welch Foundation (Grant B-1174) and the UNT Organized Research Fund.

References and Notes

(1) Børve, K. J.; Pettersson, L. G. M. *J. Phys. Chem.* **1991**, *95*, 3214.
(2) Feng, Y.; Niiranen, J.; Gutman, D. *J. Phys. Chem.* **1991**, *95*, 6564.
(3) Hutchings, G. J.; Woodhouse, J. R.; Scurrell, M. S. *J. Chem. Soc., Faraday Trans. 1* **1989**, *85*, 2507.
(4) Mehandru, S. P.; Anderson, A. B.; Brazdil, J. F.; Grasselli, R. K. *J. Phys. Chem.* **1987**, *91*, 2930.
(5) Pedley, J. B.; Naylor, R. D.; Kirby, S. P. *Thermochemical Data of Organic Compounds*; Chapman and Hall: New York, 1986; p 89.
(6) Chase, M. W., Jr.; Davies, C. A.; Downey, Jr.; Frurip, D. J.; McDonald, R. A.; Syverup, A. N. *JANAF Thermochemical Tables*; *J. Phys. Chem. Ref. Data* **1985**, *14* (Suppl. No. 1).
(7) Slavejkov, A. G.; Stanton, C. T.; Fontijn, A. *J. Phys. Chem.* **1990**, *94*, 3347 and references therein.
(8) Parnis, J. M.; Mitchell, S. A.; Kanigan, T. S.; Hackett, P. A. *J. Phys. Chem.* **1989**, *93*, 8045.
(9) Fontijn, A.; Futerko, P. M. In *Gas-Phase Metal Reactions*; Fontijn, A., Ed.; North-Holland: Amsterdam, 1992; Chapter 6.
(10) Garland, N. L.; Nelson, H. H. *Chem. Phys. Lett.* **1992**, *191*, 269.
(11) Fontijn, A.; Felder, W. In *Reactive Intermediates in the Gas Phase. Generation and Monitoring*; Setser, D. W., Ed.; Academic Press: New York, 1979; Chapter 2.
(12) Pearse, R. W. B.; Gaydon, A. G. *The Identification of Molecular Spectra*; Chapman and Hall: London, 1976; p 41.
(13) Irvin, J. A.; Quickenden, T. I. *J. Chem. Educ.* **1983**, *60*, 711.
(14) Press, W. H.; Flannery, B. P.; Teukolsky, S. A.; Vetterling, W. T. *Numerical Recipes*; Cambridge University: Cambridge, 1986; Chapter 14.
(15) Benson, S. W. *Thermochemical Kinetics*, 2nd ed.; John Wiley: New York, 1976; Chapter 4.
(16) Wagener, R.; Wagner, H. Gg. *Ber. Bunsen-Ges. Phys. Chem.* **1990**, *94*, 1096.
(17) Chu, J. O.; Beach, D. B.; Jasinski, J. M. *J. Phys. Chem.* **1987**, *91*, 5340.
(18) Becerra, R.; Frey, H. M.; Mason, B. P.; Walsh, R.; Gordon, M. S. *J. Am. Chem. Soc.* **1992**, *114*, 2752.
(19) Wentworth, W. E. *J. Chem. Educ.* **1965**, *42*, 96.
(20) Fontijn, A.; Felder, W. *J. Phys. Chem.* **1979**, *83*, 24.
(21) Frisch, M. J.; Head-Gordon, M.; Trucks, G. W.; Foresman, J. B.; Schlegel, H. B.; Raghavachari, K.; Robb, M. A.; Binkley, J. S.; Gonzalez, C.; Defrees, D. J.; Fox, D. J.; Whiteside, R. A.; Seeger, R.; Melius, C. F.; Baker, J.; Martin, R. L.; Kahn, L. R.; Stewart, J. J. P.; Topiol, S.; Pople, J. A. *Gaussian 90*; Gaussian: Pittsburgh, PA, 1990.
(22) Yu, H.; Goddard, J. D. *Can. J. Chem.* **1990**, *68*, 663.
(23) Jeong, G. H.; Klabunde, K. J. *J. Am. Chem. Soc.* **1986**, *108*, 7103.
(24) Jordan, K. D.; Kurtz, H. A. In *Metal Bonding and Interactions in High Temperature Systems*; ACS Symposium Series 179; Gole, J. L., Stwalley, W. C., Eds.; American Chemical Society: Washington, DC, 1982; Chapter 26.
(25) Oblath, S. B.; Gole, J. L. *J. Chem. Phys.* **1979**, *70*, 581; *Combust. Flame* **1980**, *37*, 293.
(26) Unscaled MP2/3-21G(*) frequencies ν for CH_3AlOH are 21, 220, 387, 520, 618, 662, 759, 935, 1322, 1549, 1559, 3054, 3130, 3155, and 3674 cm^{-1}. ν for $CH_3Al(O)H$ are 44, 192, 411, 581, 655, 744, 781, 908, 1356, 1555, 1557, 2016, 3057, 3125, and 3150 cm^{-1}; ν for CH_3OAlH are 87, 151, 242, 630, 726, 1158, 1203, 1275, 1557, 1607, 1613, 1910, 3061, 3126, and 3142 cm^{-1}. The CH_3 groups in these species are essentially free rotors.
(27) Difficulties in describing AlO with a single reference wave function make these estimates uncertain, although the energy difference between the three adducts is unaffected. See e.g.: Marshall, P.; O'Connor, P. B.; Chan, W. T.; Kristof, P. V.; Goddard, J. D. In *Gas-Phase Metal Reactions*; Fontijn, A., Ed.; North-Holland: Amsterdam, 1992; Chapter 8.
(28) (a) Dean, A. M. *J. Phys. Chem.* **1985**, *89*, 4600. (b) Westmoreland, P. R. QRRK EGA Program, 1988.